Buckling of Carbon Nanotube-Reinforced Polymer Laminated Composite Materials Subjected to Axial Compression and Shear Loadings

J. C. Riddick[1]
Vehicle Technology Directorate, U.S. Army Research Laboratory, Hampton, VA 23681

T. S. Gates[2]
NASA Langley Research Center, Hampton, VA 23681

S.-J. V. Frankland[3]
National Institute of Aerospace, 100 Exploration Way, Hampton, VA 23666

ABSTRACT

A multi-scale method to predict the stiffness and stability properties of carbon nanotube-reinforced laminates has been developed. This method is used in the prediction of the buckling behavior of laminated carbon nanotube-polyethylene composites formed by stacking layers of carbon nanotube-reinforced polymer with the nanotube alignment axes of each layer oriented in different directions. Linking of intrinsic, nanoscale-material definitions to finite scale-structural properties is achieved via a hierarchical approach in which the elastic properties of the reinforced layers are predicted by an equivalent-continuum modeling technique. Solutions for infinitely long symmetrically laminated nanotube-reinforced laminates with simply-supported or clamped edges subjected to axial compression and shear loadings are presented. The study focuses on the influence of nanotube volume fraction, length, orientation, and functionalization on finite-scale laminate response. Results indicate that for the selected laminate configurations considered in this study, angle-ply laminates composed of aligned, non-functionalized carbon nanotube-reinforced lamina exhibit the greatest buckling resistance with 1% nanotube volume fraction of 450 nm uniformly-distributed carbon nanotubes. In addition, hybrid laminates were considered by varying either the volume fraction or nanotube length through-the-thickness of a quasi-isotropic laminate. The ratio of buckling load-to-nanotube weight percent for the hybrid laminates considered indicate the potential for increasing the buckling efficiency of nanotube-reinforced laminates by optimizing nanotube size and propotion with respect to laminate configuration.

INTRODUCTION

Because of many unique mechanical and electrical properties, carbon nanotubes (CNT) have been recognized as particularly well suited for the development of nanocomposite structural materials. For applications that require thin gauge components,

---

[1]Aerospace Engineer
[2]Senior Materials Research Engineer, Mechanics of Structures and Materials Branch
[3]Senior Research Scientist

load carrying capability, and utilize minimum structural weight as a key design objective, one choice is to incorporate the CNT in a thin, polymer film or layer, to form a nanocomposite material. Potential applications for such nanostructured films include surface coatings, MEMS sensors, actuators, and gossamer or ultra-light aircraft. Experimental characterization using thermogravimetric analysis, mechanical tests, and scanning electron or probe microscopy indicates that the addition of CNT enhances mechanical properties of polymer films with respect to hardness, stiffness, and flexural strength.

Recent advances have lead to the synthesis of ultra-thin layered nancomposites. A major purpose of layering, or lamination, is to tailor the directional dependence of strength and stiffness of a material to match the loading environment of a structural element. Reference 1 discusses experimental issues related to fabrication of nanolaminates such as adsorption and dispersion. In contrast to ultra-thin carbon-fiber composites, CNT-polymer composites are considered nanostructured in the sense that the primary constituents have structure that can be readily described at the nano-scale. These material descriptions then provide the basis for the development of the underlying structure-property relationships that can be subsequently used in analysis models to tailor or enhance performance of structural components. To be truly useful, the structure-property relationships and related models must span multiple length scales and be versatile enough to be used in parametric studies that influence material development and design.

Buckling resistance is an important consideration in the design of thin-walled, lightweight aerospace vehicles and structural components. Reducing structural weight while at the same time increasing buckling capacity make composite materials, which exhibit high strength-to-weight and stiffness-to-weight ratios, ideal for aerospace vehicle structural components. Nanotube-reinforced laminated composites represent a new class of structural materials to be exploited for potential development of a variety of new, advanced applications. Ideally, longer nanotubes in high volume concentrations will offer the greatest mechanical advantage in enhancing bulk constitutive properties of matrix material. However, the current state-of-the-art in manufacturing CNT-polymer composites suggest that cost and processing issues will drive the future development CNT-reinforced laminated composite materials.

Structural tailoring of laminated composite plates has been studied extensively. Nemeth in reference 2 provides an exhaustive parametric treatment of the buckling response of symmetrically laminated fiber-reinforced panels. The detailed studies contained in this reference culminates in a set of design curves based upon the buckling behavior of infinitely long laminates. Buckling results for infintely long plates are important to designers because they provide the lower bounds to the festoon buckling curves of finite-length rectangular plates that are particularly useful in preliminary design studies. The nondimensional buckling parameters and equations presented by Nemeth have been used by Odegard, et. al.,[3] as part of a multi-scale analysis based upon a hierarchical approach used to determine the buckling resistance of single layer orthotropic composite plates subjected to uniform axial compression, uniform shear, or pure in-plane bending for CNT-reinforced composite plates. In particular, plates made of a polyethylene matrix material reinforced with single-walled carbon nanotubes were analyzed. The multi-scale analysis was used to quantify the relative influence of

molecular-level structural items defined as nanotube length, volume fraction, orientation, and functionalization on the buckling resistance of infinitely long plates. Each of the four molecular attributes considered may be controlled at material synthesis. The study found that randomly-oriented, non-functionalized nanotube-reinforcement would be recommended for single-layer plates when the design criteria is focused on providing the largest possible value for in-plane buckling resistance.

In this paper, a multi-scale analysis will be employed to predict the stiffness and stability properties of CNT-reinforced laminated composite materials. The objective of the present study is to extend the existing multi-scale analysis method of Odegard, et. al.,[3] to predict the stiffness and stability properties of a CNT-reinforced laminated composites. The multi-scale analysis concept links nanomechanics results from molecular dynamics (MD) simulations to the Mori-Tanaka micromechanics model via an equivalent-continuum modeling approach in order to predict bulk elastic properties for polymer lamina reinforced using single-walled carbon nanotubes (CNT). Herein, the CNT-dependent properties derived from the equivalent-continuum modeling approach are incorporated into traditional Classical Lamination Theory (CLT) to obtain a first-order prediction of macromechanical stiffness properties for a given CNT-reinforced laminate configuration. This method is used to facilitate the prediction of the buckling behavior of infinitely long symmetrically laminated CNT-reinforced polyethylene composites to be used in preliminary design studies. The symmetrically laminated CNT-reinforced polymer composites are formed by stacking layers with the principal material axes of each layer oriented in different directions, such that each layer located above the laminate midplane has a corresponding layer below the midplane, with the same lamina properties. For the present study lamina material properties are defined as thickness, nanotube volume fraction, length, alignment, and orientation.

Nondimensional parameters and equations that define the stiffness and stability properties of laminated plates are applied to selected laminates subjected to uniform axial compression and shear loadings. Buckling solutions for infinitely long laminates with simply-supported or clamped edges are presented. Finally, hybrid laminates are formed by varying molecular properties through-the-thickness of the laminate. The buckling response of selected hybrid laminates is presented in terms of a buckling-to-weight percent nanotube ratio. Here, buckling load is normalized by nanotube weight percent in an effort to assess the potential for tailoring the laminate response in a cost effective manner with respect to laminate configuration.

PROBLEM DESCRIPTION

A description of the multi-scale analysis is presented here. First, the material system to be analyzed is described. Then, analysis details at each length scale are outlined. Finally, the details of the hybrid laminate definition and nomenclature are presented.

Materials

The material system used in this study was a carbon nanotube-reinforced polymer composite. The carbon nanotube material was modeled as a single-walled (10,10)

nanotube of radius 6.78 Å and variable length. The polymer matrix material was assumed to be isotropic, amorphous polyethylene matrix with a representative Young's modulus and Poisson's ratio of 0.9 GPa and 0.3, respectively.

Nanomechanics

The nanotube-reinforced CNT-polymer laminates considered in the present study are considered nanostructured because the primary constituents have structure that must be analyzed at nano-scale. A nano-scale analysis[3] is employed to develop underlying structure-property relationships that can be used in analysis models to tailor or enhance performance of structural components. Highlights of the nanomechanical analysis are presented in this section.

Previous work[3] defined four nanoscale structural items as the primary molecular attributes, controlled at material synthesis, which could influence final properties of the composite. These four attributes are nanotube length, L, nanotube volume fraction, v_f, nanotube orientation, θ, and nanotube functionalization. Nanotube functionalization is defined as the formation of a chemical covalent bond between the nanotube and polymer directly. The hierarchical approach employed in the present study allows the influence of these four intrinsic attributes on bulk constitutive properties to be quantified.

The hierarchical modeling method relies on three major steps. First, molecular dynamics (MD) simulations are conducted using a suitable representative volume element (RVE) of the nanoscale molecular structure of the CNT-polymer system. Second, an equivalent-truss model is developed, using finite-element analysis, to link the MD results to an equivalent-continuum model. Finally, the equivalent-continuum model is developed to model the nanotube as an effective fiber. The effective mechanical properties of the molecular system are determined by equating the strain energies of the molecular and equivalent-continuum models. The equivalent-continuum–effective-fiber results yield the nine independent elastic constants used to describe the overall of the behavior of the effective fiber: three elastic axial stiffnesses, C_{11}^f, C_{22}^f, and C_{33}^f; the plane-strain bulk moduli, K_{23}^f, K_{13}^f, and K_{12}^f; and the three elastic shear stiffnesses, C_{44}^f, C_{55}^f, and C_{66}^f. Where, the subscripts 1, 2, 3 indicate principal material directions; subscripts 4, 5 and 6 are indices of the stiffness tensor written in Voigt's notation; and the superscript f denotes that these properties are associated with the effective fiber.

Table 1. Equivalent-Continuum Properties (GPa).

	Non-functionalized effective fiber	Functionalized effective fiber
C_{11}^f	548.7	487.7
C_{22}^f	16.8	24.5
C_{33}^f	16.5	20.6
K_{23}^f	14.8	19.5
K_{13}^f	149.3	137.1
K_{12}^f	149.2	138.7
C_{44}^f	7.1	12.7
C_{55}^f	144.0	155.4
C_{66}^f	144.9	137.0

The nine independent elastic properties given in Table 1 are determined by applying nine identical sets of boundary conditions to the equivalent-truss model and the equivalent-continuum model. The strain energies of the models are equated by adjusting the elastic properties in a parametric fashion. Table 1 presents the nine independent parameters, where functionalized and non-functionalized nanotube systems were modeled as effective fibers.

Micromechanics

Constitutive models governing the behavior of nanotube-reinforced polymer lamina were obtained from a micromechanical analysis by using the mechanical properties of effective fibers.[3] In this analysis, the polymer molecules near the polymer/nanotube interface were included in the effective fiber, and it was assumed that the polymer matrix surrounding the effective fiber had mechanical properties equal to those of bulk polyethylene. Perfect bonding between the nanotube/polymer effective fibers and the surrounding polymer matrix was also assumed.

A micromechanics-based Mori-Tanaka method was used to predict the elastic mechanical properties of the composite material.[3] For this method, the overall elastic-stiffness tensor of the nanotube-reinforced lamina composed of CNT embedded in a matrix material is

$$\mathbf{C} = \left(v_m \mathbf{C}_m + v_f \left\langle \mathbf{C}_f \mathbf{T}_f \right\rangle \right) \left(v_m \mathbf{I} + v_f \left\langle \mathbf{T}_f \right\rangle \right)^{-1} \tag{1}$$

where v_f and v_m are the effective fiber and matrix volume fractions, respectively, $\mathbf{C}_f$ and $\mathbf{C}_m$ are the stiffness tensors of the effective fiber and the matrix respectively, $\mathbf{I}$ is the identity tensor, the angle brackets indicate an effective-fiber orientation average, and $\mathbf{T}_f$ is the dilute strain-concentration tensor of the effective fiber, and is given by

$$\mathbf{T}_f = \left[\mathbf{I} + \mathbf{S} \mathbf{C}_m^{-1} \left(\mathbf{C}_f - \mathbf{C}_m \right) \right]^{-1} \tag{2}$$

where $\mathbf{S}$ is the Eshelby13 tensor.

Lamina properties, namely the Young's and shear moduli are determined using the homogenized-composite stiffness tensor, $\mathbf{C}$. The shear moduli of the composite material (G_{23}, G_{31}, G_{12}) are simply equal to the shear-stiffnesses (C_{44}, C_{55}, C_{66}), the Young's moduli (E_1, E_2, E_3) were calculated by using the components of the compliance tensor of the nanotube-reinforced lamina determined by inverting the composite stiffness tensor $\mathbf{C}$.[15] For composite lamina composed of aligned CNT, the subscripts of the Young's and shear moduli indicate the principal direction associated with the quantity. Where the 1-direction is parallel to the longitudinal axis of the nanotube, the orthogonal 2- and 3-directions are transverse to the logitudnal axis of the nanotube. For the random-oriented composite lamina, isotropic mechanical properties are completely described by the Young's modulus, E ($E = E_1 = E_2 = E_3$) and shear modulus, G ($G = G_{23} = G_{31} = G_{12}$).

For the present study, lamina properties were determined using the elastic stiffness components, volume fraction, length, and orientation of the effective fiber properties in Eq. (1). The calculations were performed for perfectly aligned and three-dimensional

randomly oriented effective fibers. Symmetrically laminated CNT-reinforced polymer composites are formed by stacking lamina with the principal material axes of each layer oriented in different directions in a manner that maintains the symmetry about the laminate midplane, as depicted in Figure 1.

Macromechanics

The buckling analysis is based on the classical Rayleigh-Ritz variational method and is derived explicitly in terms of the nondimensional parameters defined in Reference 2. Deriving the analysis in this manner produces equations well-suited for parametric studies. The nondimensional parameters used are given by

$$\beta = \frac{D_{12} + D_{66}}{\sqrt{D_{11}D_{22}}} \tag{3}$$

$$\gamma = \frac{D_{16}}{\left(D_{11}^3 D_{22}\right)^{1/4}} \tag{4}$$

$$\delta = \frac{D_{26}}{\left(D_{11}D_{22}^3\right)^{1/4}} \tag{5}$$

Where, the parameter β characterizes plate bending orthotropy, and δ and γ characterize plate bending anisotropy. The subscripted D terms appearing in the equations are the plate bending bending stiffnesses of Classical Lamination Theory (CLT)[4] defined as

$$D_{ij} = \frac{1}{3}\sum_{k=1}^{N}\left(\overline{Q}_{ij}\right)_k\left(z_k^3 - z_{k-1}^3\right) \tag{6}$$

where k, N, z_k, and z_{k-1} are defined in Figure 1, $\overline{Q}_{ij}$ represent the transformed reduced stiffnesses for each lamina as defined in Reference 4. For aligned nanotubes, the transformed reduced stiffness matrix is dependent on the nanotube orientation angle and the four independent elastic constants E_1, E_2, G_{12}, and ν_{12}. For lamina reinforced by randomly-oriented nanotubes, the transformed reduced stiffnesses reduce to the isotropic formulation presented by Odegard, et. al.[3] Note that all of the parameters defined by equations (3) through (5) depend on plate bending stiffnesses which can be shown to be functions of the lamina elastic properties and nanotube orientation. The lamina constitutive properties and nanotube orientation are functions of the intrinsic molecular properties. Therefore, the bending stiffness, and furthermore the parameters of equations (3) through (5), may be expressed as functions of the intrinsic molecular properties.

In addition to β, δ, and γ, two additional nondimensional quantities are used to characterize buckling resistance, and they are given by

$$K_x = \frac{N_x^{cr} b^2}{\pi^2 \sqrt{D_{11} D_{22}}} \qquad (7)$$

$$K_s = \frac{N_{xy}^{cr} b^2}{\pi^2 \sqrt{D_{11} D_{22}}} \qquad (8)$$

The quantities K_x and K_s are referred to as the axial compression buckling coefficient and the shear buckling coefficient, respectively. Each of the loading conditions associated with these buckling coefficients is shown in Figure 2. The compressive and shear stress resultants corresponding to the loadings are denoted by N_x and N_{xy}, respectively. All stress resultants shown are positive-valued. The superscript cr denotes the critical value of the applied load associated with the onset of buckling. Finally, the laminate width, b, is defined in Figure 2.

A set of simplified buckling equations are presented in Table 2 which were determined by performing a least squares fit to response curves determined by a special-purpose Rayleigh-Ritz analysis. Nemeth[2] provides the following simplified linear expressions for the buckling coefficients:

Table 2. Buckling coefficients for in-plane loading.

	Simply-supported edges	clamped edges
K_x	$2 + 2\beta$	$4.602 + 2.359\beta$
K_s	$3.629 + 1.644\beta$	$6.493 + 2.414\beta$

The equations for the buckling coefficients given in Table 2 depend only on nondimensional parameter β. These equations arise from an analysis that neglects the effect of laminate bending anisotropy. According to Reference 5, the bending anisotropy is expected to be negligible when the maximum value of nondimensional anisotropy parameters δ and γ are less than 0.2. A potential benefit of certain symmetric laminate configurations is a high degree of bending anisotropy. Such categories of laminates could potentially give rise to δ and γ values in excess of 0.2. Therefore, care must be taken in choosing laminates to be analyzed using these buckling equations.

The potential tailoribility of the buckling behavior of nanotube-reinforced polymer composites will be assessed by studying the effects of fiber orientation, stacking sequence and intrinsic molecular properties on the nondimensional parameters and buckling coefficients. In the analysis two major categories of laminates are considered: (1) laminates with a constant nanotube volume fraction of 1% in which nanotube length is varied from 3 nm to 450 nm, and, (2) laminates with consisting of a constant a nanotube length of 400 nm in which nanotube volume fraction is varied from 1% to 20%. In the first category of laminates, shorter 3-nm nanotubes represent the current state-of-the-art, while longer 450-nm represent future technological goals. For the second category of laminates, volume fractions less than 5% represent the current state-of-the-art

and volume fractions above 5%, while perhaps ideal, are in most cases too expensive or physically not practical.

Hybrid Laminates

Figure 3 shows a schematic of typical layups for uniform and hybrid angle-ply [+45/-45]$_s$ laminates. In the uniform laminate, the intrinsic molecular properties are constant throughout the laminate. By contrast, the hybrid laminate allows that the lamina properties may be alternated by varying the lamina molecular properties in a manner which adheres to laminate symmetry. Here, nanotube length, L, and volume fraction, v_f, may vary about the midplane only if each layer located above the laminate midplane has an equivalent counterpart below the midplane. Table 3 shows a series of hybrid laminates of the [$\pm45/0/90$]$_{ms}$ family of laminates.

Table 3. Quasi-isotropic hybrid [±45/0/90]ms laminate configurations.

Laminate number	Fixed lamina properties	Laminate configuration
1	$v_f = 1\%$	$[(\pm45/0/90)_3{}^{L=10\text{nm}}/(\pm45/0/90)_3{}^{L=\lambda}]_s$
2	$v_f = 1\%$	$[(\pm45/0/90)_3{}^{L=400\text{nm}}/(\pm45/0/90)_3{}^{L=\lambda}]_s$
3	$v_f = 1\%$	$[(\pm45/0/90)_3{}^{L=\lambda}/(\pm45/0/90)_3{}^{L=400\text{nm}}]_s$
4	$v_f = 1\%$	$[(\pm45/0/90)_3{}^{L=\lambda}/(\pm45/0/90)_3{}^{L=10\text{nm}}]_s$
5	$L = 400$ nm	$[(\pm45/0/90)_3{}^{vf=1\%}/(\pm45/0/90)_3{}^{vf=\phi}]_s$
6	$L = 400$ nm	$[(\pm45/0/90)_3{}^{vf=10\%}/(\pm45/0/90)_3{}^{vf=\phi}]_s$
7	$L = 400$ nm	$[(\pm45/0/90)_3{}^{vf=\phi}/(\pm45/0/90)_3{}^{vf=10\%}]_s$
8	$L = 400$ nm	$[(\pm45/0/90)_3{}^{vf=\phi}/(\pm45/0/90)_3{}^{vf=1\%}]_s$

For each hybrid laminate configuration either nanotube length or volume fraction is fixed for the entire laminate. Also, the nanotube, length or volume fraction is fixed for groupings of lamina with a laminate denoted by the superscript within the laminate configuration. The nanotube length or volume fraction of the remaining groups of lamina may be assigned by varying the nanotube length and volume fraction parameters λ and ϕ, respectively, thus allowing parametric studies. For example, the hybrid quasi-isotropic $[(\pm45/0/90)_3{}^{L=400\text{nm}}/(\pm45/0/90)_3{}^{L=\lambda}]_s$ laminate, identified in Table 3 as laminate 2, has a constant volume fraction of 1% . The 3 outer ($\pm45/0/90$) groups on either side of the midplane are reinforced by 400-nm nanotubes, while the nanotube lengths of the inner ($\pm45/0/90$) groups may be assigned uniformly be varying the nanotube length parameter λ. For the present study, λ will be varied between 3 nm and 450 nm, and ϕ will be varied between 1% and 20%.

RESULTS AND DISCUSSION

The buckling behavior of nanotube-reinforced polymer laminated composites will be assessed by presenting data showing the effects of stacking sequence and intrinsic molecular properties on the nondimensional parameters and buckling coefficients. Results are presented in this section for angle-ply $[\pm\theta]_{ms}$; quasi-isotropic $[\pm45/0/90]_{ms}$; axially-stiff $[\pm45/0_2]_{ms}$; and transversely-stiff $[\pm45/90_2]_{ms}$ laminates. Also, to investigate the potential for optimizing the weight efficiency of such laminates, results depicting the effect of hybrid laminate configurations on the ratio of axial buckling load-to-nanotube weight percent are presented.

Results showing the effects of varying nanotube length and volume fraction on the nondimensional bending orthotropy parameter β for quasi-isotropic $[\pm45/0/90]_s$ laminates are presented in Figures 4(a) and 4(b). In Figure 4(a), nanotube length is varied uniformly for a constant 1% nanotube volume fraction. In Figure 4(b), nanotube volume fraction is varied uniformly where all plies are reinforced by 400-nm nanotubes. Both Figures 4(a) and 4(b) present results for quasi-isotropic laminates composed of aligned, randomly oriented, functionalized and non-functionalized nanotubes in various combinations.

The results presented in Figure 4(a) indicate that for 1% volume fraction quasi-isotropic $[\pm45/0/90]_s$ laminates composed of functionalized and non-functionalized randomly-oriented nanotube-reinforced plies, the value of the nondimensional parameter β remains nearly constant over a range of nanotube lengths varying from 3 nm to 450 nm. In contrast, the data shows that for 1% nanotube volume fraction $[\pm45/0/90]_s$ laminates composed of aligned functionalized and non-functionalized nanotubes, the value of β increases monotonically over the same range of nanotube lengths. The results for aligned non-functionalized CNT-reinforced laminates show a slightly larger value at the maximum nanotube length of 450 nm compared to the functionalized nanotube result.

The results presented in Figure 4(b) indicate that for quasi-isotropic $[\pm45/0/90]_s$ laminates composed of 400-nm nanotubes, randomly-oriented functionalized and non-functionalized nanotube reinforcement yield a near constant response over a range of nanotube volume fractions increasing from 0% to 20%. By contrast, the results of Figure 4(b) indicate that the $[\pm45/0/90]_s$ laminates composed of aligned functionalized and non-functionalized nanotubes show a nearly exponential increase in β as a function of volume fraction to a maximum at 5% nanotube volume fraction. As volume fraction increases beyond 5%, β remains nearly constant.

The results of Figure 4, indicate the effect of intrinsic molecular properties on the orthotropy of nanotube-reinforced quasi-isotropic $[\pm45/0/90]_s$ laminate. In particular, results indicate in comparison to randomly-oriented nanotube-reinforced $[\pm45/0/90]_s$ laminates, aligned nanotube reinforcement yields larger values of the nondimensional bending orthotropy parameter β. For both randomly-oriented and aligned nanotube reinforcement, functionalization has little effect on the degree of orthotropy.

Figure 5 presents results that illustrate the effect on the nondimensional bending orthotropy parameter β due to varying nanotube length and volume fraction in axially-stiff $[\pm45/0_2]_s$ and $[\pm45/0_2]_{6s}$; transversely-stiff $[\pm45/90_2]_s$ and $[\pm45/90_2]_{6s}$; quasi-isotropic $[\pm45/0/90]_s$ and $[\pm45/0/90]_{6s}$; and angle-ply $[\pm45]_s$, $[\pm45]_{6s}$, $[\pm30]_{6s}$, and $[\pm60]_{6s}$ laminates. The data shown in Figure 5(a) results from varying nanotube length for uniform laminates with 1% nanotube volume fraction. Figure 5(b) shows results of

varying nanotube volume fraction for uniform laminates composed of 400-nm nanotubes. The results presented are for aligned, non-functionalized nanotubes.

In Figure 5(a), the data shown indicates that for all laminates considered the nondimensional parameter β increases monotonically as nanotube length in the uniform laminate increases from 3 nm to 450 nm. For the 3 nm nanotube length, the quasi-isotropic axially-stiff and transversely-stiff laminates share the maximum value of β and the $[\pm45]_s$ and $[\pm45]_{6s}$ angle-ply laminates share the minimum value. As the nanotube length increases uniformly to 100 nm, the values of the orthotropy parameter β for all of the laminates coalesce around unity. As the nanotube length approaches 450 nm, the maximum and minimum values of β correspond to angle-ply $[\pm45]$ family of laminates and quasi-isotropic $[\pm45/0/90]_{6s}$, respectively.

The results shown in Figure 5(b) indicate a similar trend in the data for the laminate configurations, where a uniform nanotube length of 400 nm is maintained in each layer as nanotube volume fraction is varied from 0% to 20%. Here, the data coalesces around unity at about 1% volume fraction. At a nanotube volume fraction of about 5%, the maximum and minimum values of β correspond to angle-ply $[\pm45]_s$ and $[\pm45]_{6s}$ laminates and $[\pm45/0/90]_{6s}$, respectively. The values of β remains nearly constant over the range of volume fraction values from 5% to 20%.

The results in Figure 5 indicate that for aligned, non-functionalized nanotube reinforcement the orthtropy for selected uniform laminates increases monotonically as nanotube length is increased for uniform 1% volume fraction laminates and as nanotube volume fraction is increased for uniform laminates composed of 400-nm nanotubes. The results show five distinct groupings of laminates that share orthotropy values: (1) $[\pm45]_s$ and $[\pm45]_{6s}$; (2) $[\pm30]_{6s}$, and $[\pm60]_{6s}$; (3) $[\pm45/90_2]_s$, $[\pm45/0_2]_s$, and $[\pm45/0/90]_s$; (4) $[\pm45/0_2]_{6s}$ and $[\pm45/90_2]_{6s}$; and (5) $[\pm45/0/90]_{6s}$. These groupings of laminates are each represented by a line in the plots of Figures 5(a) and 5(b). The data in both Figures show that varying the intrinsic molecular properties significantly alters the degree of orthotropy among the uniform laminates studied. Namely, trends in orthotropy associated with laminate configuration reverse themselves as nanotube length or volume fraction is increased. Thus, the maximum value of β among the uniform laminates considered can be tailored by varying the intrinsic molecular properties of the nanotube used to reinforce the laminates.

Nondimensional buckling coefficients for axial compression and shear loadings, K_x and K_s, respectively, for a quasi-isotropic $[\pm45/0/90]_{6s}$ uniform laminate are shown in Figure 6. Results are shown for both simply-supported and clamped boundary conditions. The nondimensional buckling coefficients are presented as functions of nanotube length for a constant 1% volume fraction for aligned, non-functionalized carbon nanotubes in Figure 6(a). While, Figure 6(b) shows nondimensional buckling results as a function of nanotube volume fraction for 400-nm aligned, non-functionalized CNT reinforcement.

In Figure 6(a), the axial buckling coefficient and shear buckling coefficient, K_x and K_s, respectively, for the uniform quasi-isotropic $[\pm45/0/90]_{6s}$ laminate both show a slight increase over the range of nanotube length from 3nm to 450 nm. The clamped and simply-supported results show the same trend. For both buckling coefficients K_x and K_s, the simply-supported results, represented by the dashed lines, have greater values than the clamped results. Values of the shear buckling coefficient K_s are shown to exceed values of the axial buckling coefficient K_x over the entire range of nanotube lengths.

A similar trend is observed in the buckling results presented as a function of nanotube volume fraction shown in Figure 6(b). Here, the response of a uniform quasi-isotropic [±45/0/90]$_{6s}$ laminate is considered for a 400-nm aligned, non-functionalized nanotube reinforcement by varying nanotube volume fraction from 0% to 20%. Both buckling coefficients K_x and K_s increase slightly over the range of nanotube volume fractions. The results for both the clamped and simply-supported boundary conditions show the same trends as functions of volume fraction. The simply-supported results, represented by the dashed lines, are greater than the buckling coefficient values for the clamped boundary conditions. Also, the value of the shear buckling coefficient K_s is shown to exceed the values of the axial buckling coefficient K_x for entire range of nanotube volume fractions.

Buckling results presented in Figure 6 for the uniform quasi-isotropic [±45/0/90]$_{6s}$ for aligned, non-functionalized CNT show that buckling response is a function of loading and boundary conditions. For a particular laminate, trends in the buckling results for axial compression and shear loadings are similar. Furthermore results for both simply-supported of clamped boundary conditions are similar.

Buckling results for simply-supported uniform axially-stiff [±45/0$_2$]$_{6s}$; transversely-stiff [±45/90$_2$]$_{6s}$; quasi-isotropic [±45/0/90]$_{6s}$; and angle-ply [±45]$_{6s}$ laminates reinforced with aligned, non-functionalized CNT are presented in Figures 7 and 8. Results for the axial buckling coefficient K_x are presented in Figure 7 as a function of nanotube length for a constant 1% volume fraction. In Figure 8, the shear buckling coefficient results as a function of nanotube volume concentration are presented for a 400-nm CNT.

Figure 7 shows that for 1% nanotube volume fraction, at a nanotube length of 3nm, the uniform angle-ply [±45]$_{6s}$ laminate has the lowest axial buckling coefficient, while the uniform axially-stiff [±45/0$_2$]$_{6s}$, transversely-stiff [±45/90$_2$]$_{6s}$, and quasi-isotropic [±45/0/90]$_{6s}$ laminates share the same value. As nanotube length increases the value of the buckling coefficients increase monotonically. At around 150 nm, the value of the buckling coefficient for the [±45]$_{6s}$ laminate becomes largest. Finally, at 450 nm, the [±45]$_{6s}$ laminate has the maximum value, the [±45/0$_2$]$_{6s}$ and [±45/90$_2$]$_{6s}$ share the same value, and the [±45/0/90]$_{6s}$ has the lowest value.

A similar trend for the shear buckling coefficient for 400-nm aligned, non-functionalized nanotube reinforcements over a range of nanotube volume fractions from 0% to 20% is shown in Figure 8. At 0%, the [±45]$_{6s}$ laminates have the shear buckling coefficient, while the uniform [±45/0$_2$]$_{6s}$, [±45/90$_2$]$_{6s}$, and [±45/0/90]$_{6s}$ laminates share the same greater value. As nanotube volume increases the value of the shear buckling coefficients increase monotonically. At around 2% nanotube volume fraction, the value of the shear buckling coefficient for the [±45]$_{6s}$ laminate becomes largest. Over the range of nanotube volume fractions from 5% to 20%, the [±45]$_{6s}$ laminate has the maximum value, the [±45/0$_2$]$_{6s}$ and [±45/90$_2$]$_{6s}$ share the same value, and the [±45/0/90]$_{6s}$ has the lowest value.

The results of Figures 7 and 8 show that the intrinsic molecular properties may have a significant effect on the buckling response of certain nanotube-reinforced laminates exposed to axial compression and shear loadings. In particular, buckling coefficient values of the uniform angle-ply [±45]$_{6s}$ laminate ranged from minimum to maximum in both axial compression and shear buckling response over a range of nanotube length and volume fraction values for aligned, non-functionalized carbon nanotube reinforcement. The increase in buckling load due to variation in nanotube proportion and size suggest the

potential to tailor the buckling response of the laminate to various loading conditions using the molecular properties of the nanotubes.

Figure 8 presents buckling results for the hybrid quasi-isotropic $[\pm 45/0/90]_{6s}$ family of CNT-reinforced laminates subjected to axial compressive loadings. These laminates are considered hybrid due to the fact that the molecular properties of the aligned, non-functionalized CNT reinforcement are varied through-the-thickness of the laminates in a manner similar to that shown in Figure 3. The laminates considered are listed in Table 3. Here, the buckling results are presented as a ratio of axial buckling load-to-nanotube weight percent. The data is normalized by the ratio of axial buckling load-to-nanotube weight percent ratio for a uniform quasi-isotropic $[\pm 45/0/90]_{6s}$ laminate.

Figure 8(a) shows the ratio of buckling load-to-nanotube weight percent for hybrid laminates 1-4 in Table 3, where the nanotube length parameter λ is varied from 3 nm to 450 nm for a constant nanotube volume fraction of 1%. Here, the results are presented as a function of nanotube length. The data is normalized by a uniform quasi-isotropic $[\pm 45/0/90]_{6s}$ laminate with a constant 1% volume. As the nanotube length is increased, the hybridized layers in the laminate remain at a constant value denoted by the superscripts in the laminate configuration notation as described previously. The results in Figure 8(a) show that, in comparison to the uniform $[\pm 45/0/90]_{6s}$ laminate, hybrid laminates 2 and 3, where the hybrid layers are fixed at 400 nm, exhibit a higher buckling load-to-nanotube weight percent ratio value for a $\lambda = 10$ nm. Laminates 1 and 4, where the hybrid layers are fixed at 10 nm, share buckling coefficient values with the uniform laminate at $\lambda = 10$ nm. As the nanotube length in the variable layers increases, the normalized buckling load-to-nanotube weight percent ratio for hybrid laminates 2 and 3 approaches unity, while the values for laminates 1 and 4 decrease to values less than unity. At the maximum nanotube length analyzed, 450 nm, laminate 1 has the the smallest buckling load-to-nanotube weight percent ratio.

All laminates in Figure 8(a) have a constant nanotube volume fraction of 1%. Therefore, in laminates 2 and 3 the increase in axial buckling capacity relative to the volume of nanotubes achieved at $\lambda = 10$ nm constitutes an enhancement in buckling performance without adding mass. Furthermore, utilizing hybrid layers away from the midplane appears to offer the greatest advantage. At $\lambda = 10$ nm, laminate 2 shows the largest increase in the normalized axial buckling load-to-nanotube weight percent ratio.

Figure 8(b) shows the normalized ratio of buckling load-to-nanotube weight percent for hybrid laminates 5-8 in Table 3, where the nanotube volume fraction parameter ϕ is varied from 1% and 20% for constant nanotube length of 400 nm. Here, the results are presented as a function of nanotube volume fraction. The data is normalized by a uniform $[\pm 45/0/90]_{6s}$ laminate composed of 400 nm nanotubes. The results for laminates 5 and 8 coincide with unity at 1% volume fraction. The results for laminates 6 and 7 coincide with unity at 10% volume fraction. This indicates that these laminates have the same volume fraction and buckling response as the uniform laminate at these points. However, for laminates 5 and 8, as the volume fraction parameter is increased, the normalized ratio of buckling load to weight percent nanotubes increases over the range of volume fraction values. At $\phi = 5\%$, laminate 5 has the maximum value at 1.7. Laminate 8 reaches a value just below 1.7 at $\phi = 5\%$. This slight difference is due to the fact that the fixed 1% volume fraction layers are placed at the midplane in laminate 8 and at the outer surface in laminate 5. More importantly the results shown reflects a 70% improvement in

the buckling load-to-weight percent ratio due to the reduction in overall nanotube volume fraction in the laminate. For $\phi > 5\%$ there is little change in the value of the buckling load-to-nanotube weight percent ratio. Also, for laminates 6 and 7, the load to weight percent ratio ranges from 0.2 at $\phi = 1\%$ to 1.25 at $\phi = 20\%$. The maximum value for laminates 6 and 7 represents a 25% increase in the load to weight percent ratio.

The results of Figure 8(b) demonstrate the fact that the axial buckling load-to-weight percent ratio can be improved by varying the nanotube volume fraction through-the-thickness of a laminate. Fixing the hybrid layers at 1% volume fraction yielded increases in the buckling load-to-nanotube weight percent ratio across a range of volume fractions from 1% to 20%. Fixing the volume fraction in hybrid layers at 10% yielded increases in the load to weight percent ratio across a range of volume fractions from 10% to 20%. Placing the hybrid layers away from the midplane offered a slight improvement in the case of the 1% volume fraction hybrid layers, but not so with the 10% hybrid layers. The hybrid laminates with fixed 1% nanotube volume fraction layers offered the maximum buckling load-to-nanotube weight percent improvement of 70% compared to the uniform laminate. The results suggest that the weight efficiency of the nanotube-reinforced laminates can be improved by optimizing the nanotube volume fraction with respect to laminate configuration. Furthermore, the optimal buckling load-to-nanotube weight percent ratio can be achieved using low nanotube volume fractions.

SUMMARY AND CONCLUSIONS

An analysis to predict the effect of intrinsic molecular properties on the buckling response of polyethylene composites reinforced by CNT subjected to axial compression and in-plane shear loadings has been conducted. The results indicate the potential for tailoring the macromechanical response of the CNT-reinforced laminates built by layering of plies or lamina of polyethylene matrix material reinforced by CNT suspended in the matrix. The buckling response of layered polyethylene CNT-reinforced laminates was demonstrated by developing a model to predict the critical buckling response of the symmetric laminates based upon the intrinsic molecular properties of the nanotube length, volume fraction, orientation, and functionalization.

Results indicate in comparison to uniform randomly-oriented CNT-reinforced quasi-isotropic [±45/0/90]$_s$ laminates, aligned nanotube reinforcement yields larger values of the nondimensional bending orthotropy parameter β. For both randomly-oriented and aligned nanotube reinforcement functionalization has little effect on the degree of orthotropy. For aligned, non-functionalized nanotube reinforcement the orthtropy for selected uniform laminates increases monotonically as nanotube length is increased for 1% volume fraction laminates and as nanotube volume fraction is increased for laminates composed of 400-nm nanotubes. The results show distinct groupings of laminates that share orthotropy values. Varying the intrinsic molecular properties significantly alters the degree of orthotropy among the uniform laminates studied. Namely, trends in orthotropy associated with laminate configuration reverse themselves as nanotube length or volume fraction is increased. Increasing volume fraction of shorter nanotubes or increasing nanotube length for low volume fraction composites gives rise to trends in laminate bending orthotropy similar to those encountered in fiber-reinforced polymer composites.

Buckling results show that buckling response is a function of loading and boundary conditions. For a particular laminate, trends in the buckling results for axial compression and shear loadings are similar. Furthermore results for both simply-supported of clamped boundary conditions are similar. Results show that the intrinsic molecular properties may have a significant effect on the buckling response of certain CNT-reinforced laminates. In particular, among a set of selected laminates configurations, buckling coefficient values of the uniform angle-ply $[\pm45]_{6s}$ laminate ranged from minimum to maximum in both axial compression and shear buckling response over a range of nanotube length and volume fraction values for aligned, non-functionalized CNT reinforcement. The increase in buckling load due to variation in nanotube proportion and size suggest the potential to tailor the buckling response of the laminate using the molecular properties of the nanotubes.

Finally, analysis of the hybrid laminate configurations showed increases in axial buckling load may be achieved without adding mass by varying the nanotube length through-thickness. Futhermore, utilizing hybrid layers away from the midplane appears to offer the greatest advantage. For $\lambda = 10$ nm, $[(\pm45/0/90)_3^{L=400nm}/(\pm45/0/90)_3{}^{L=\lambda}]_s$ shows a 15% increase in the normalized buckling load-to-nanotube weight percent ratio compared to a uniform $[\pm45/0/90]_{6s}$ laminate. By contrast, $[(\pm45/0/90)_3^{L=\lambda}/(\pm45/0/90)_3^{L=400nm}]_s$ shows only a 7% increase. Results indicate that while longer nanotubes may be optimal for mechanical properties in a generic sense, a mix of long and short nanotubes may be optimal for enhancing buckling performance. Other results indicate that the axial buckling load-to-nanotube weight percent ratio can be improved by hybridizing the nanotube volume fraction of the laminate. The hybrid $[(\pm45/0/90)_3^{vf=1\%}/(\pm45/0/90)_3{}^{vf=\phi}]_s$ laminate offered the maximum buckling to weight percent improvement of 70% at $\phi = 5\%$ compared to the uniform quasi-isotropic laminate indicating that the volume fraction, and therefore cost, maybe optimized with respect to laminate configuration to enhance buckling performance at nanotube volume fractions less than 5%.

REFERENCES

1. Rouse, JH, Lillehei, PT, Sanderson, J, Siochi, EJ, "Polymer/Single-Walled Carbon Nanotube Films Assembled via Donor-Acceptor Interactions and Their Use as Scaffolds for Silica Deposition", *Chemical Materials*, Vol. 16, pp. 3904-3910, 2004

2. Nemeth, MP, "Buckling Behavior of Long Anisotropic Plates Subjected to Combined Loads", NASA TP-3568, NASA Langley Research Center, Hampton, VA, Nov 1995

3. Gates, TS, GM Odegard, MP Nemeth, S-JV Frankland, "Predicting the Influence of Nano-scale Material Structure on the In-plane Buckling of Orthotropic Plates, AIAA Paper No. 2004-1607, in the proceedings of the 45th AIAA/ASME/ASCE/AHS Structures, Structural Dynamics, and Materials Conference, Palm Springs, CA, Apr 2004

4. Jones, RM, *Mechanics of Composite Materials*, Taylor and Francis, New York, 1998
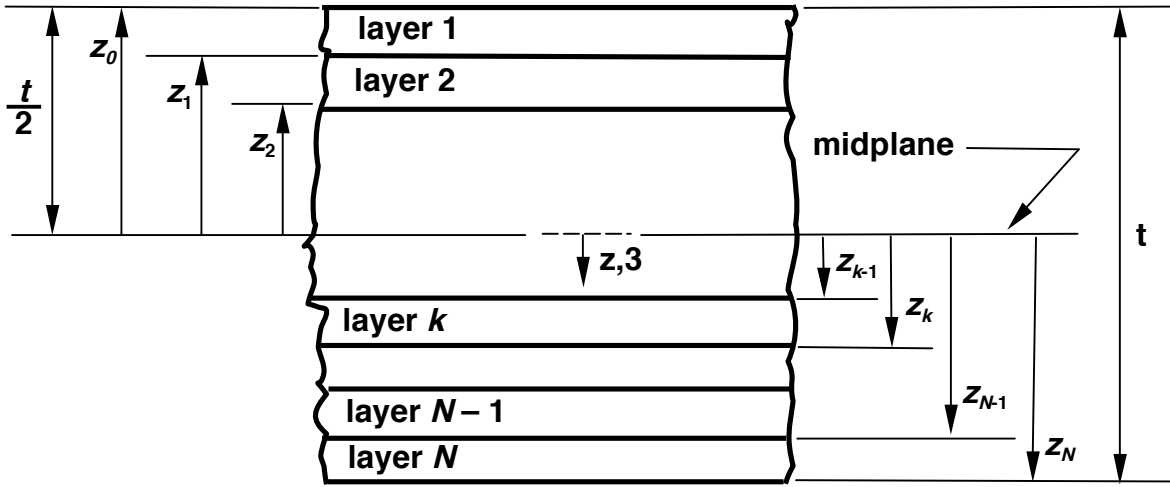
Note: For $k = 1, N$, $z_{k-1} - z_k \equiv$ constant

Figure 1. Geometry of N-layered laminate.
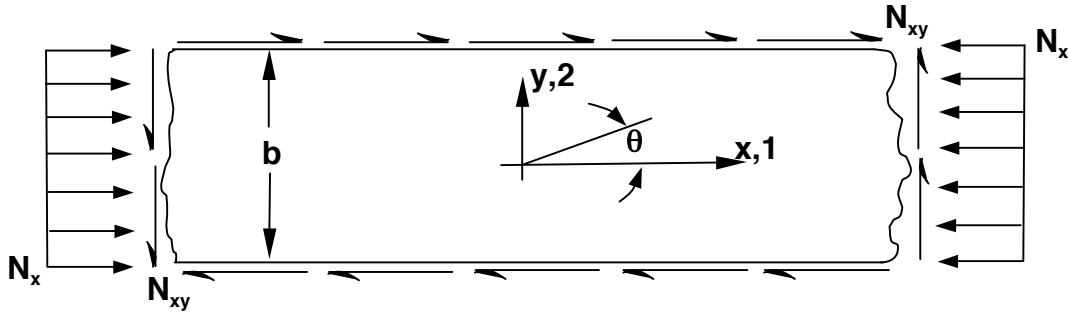
Figure 2. Geometry of infinitely long symmetric laminate subjected to axial compression and shear loadings.

Uniform   **Hybrid**

Layer 1 —— v_f +45° L ——   Layer 1 —— v_{f1} +45° L_1 ——
     2 —— v_f -45° L ——   2 —— v_{f2} −45° L_2 ——
- **midplane** -
     3 —— v_f -45° L ——   3 —— v_{f3} -45° L_3 ——
     4 —— v_f +45° L ——   4 —— v_{f4} +45° L_4 ——

Note: v_f, nanotube volume fraction; θ, nanotube orientation angle; and L, nanotube length

Figure 3. Schematic of typical $[\pm 45]_s$ uniform and hybrid symmetric laminates.

(a) 1% nanotube volume fraction

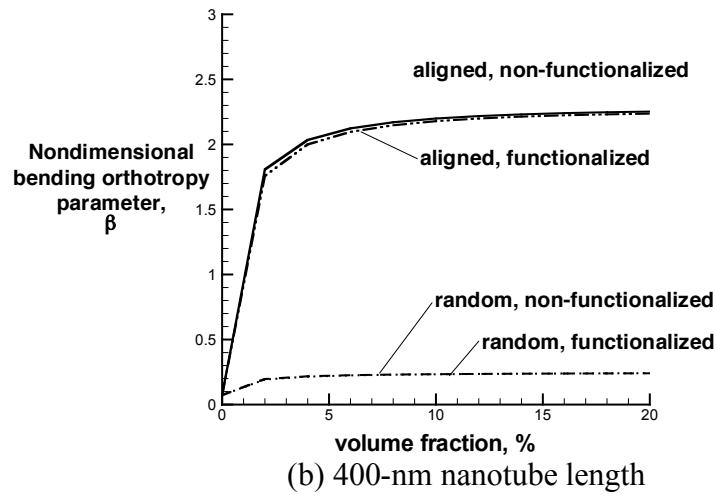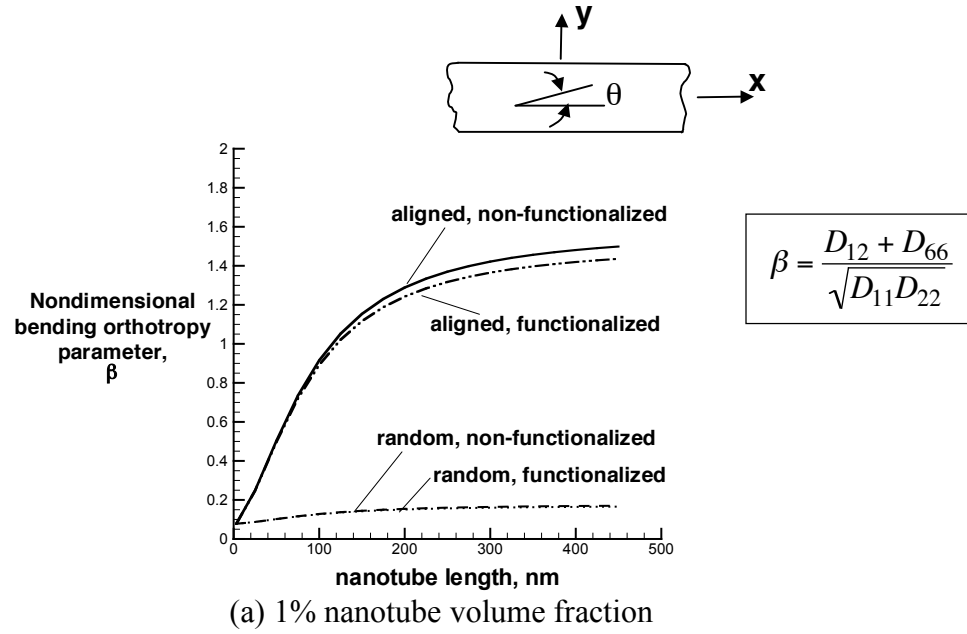$$\beta = \frac{D_{12} + D_{66}}{\sqrt{D_{11}D_{22}}}$$

(b) 400-nm nanotube length

Figure 4. Effect of intrinsic molecular properties on non-dimensional bending orthotropy parameter, β, for [±45/0/90]$_s$ laminates.

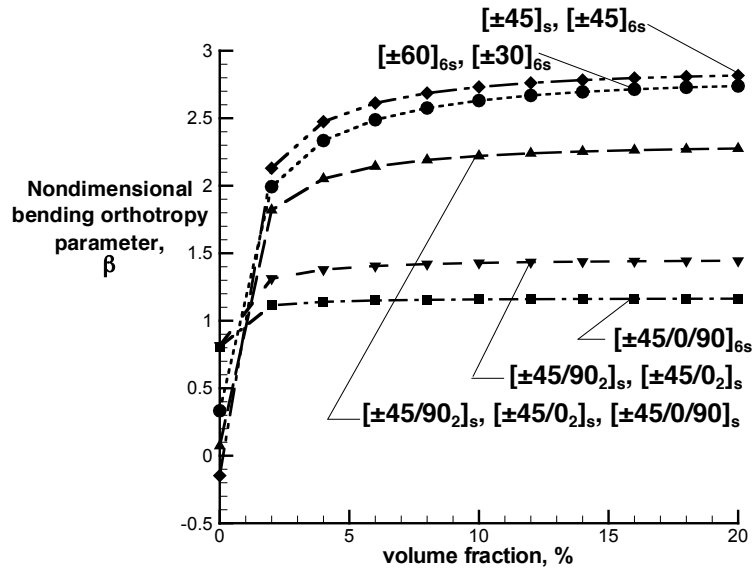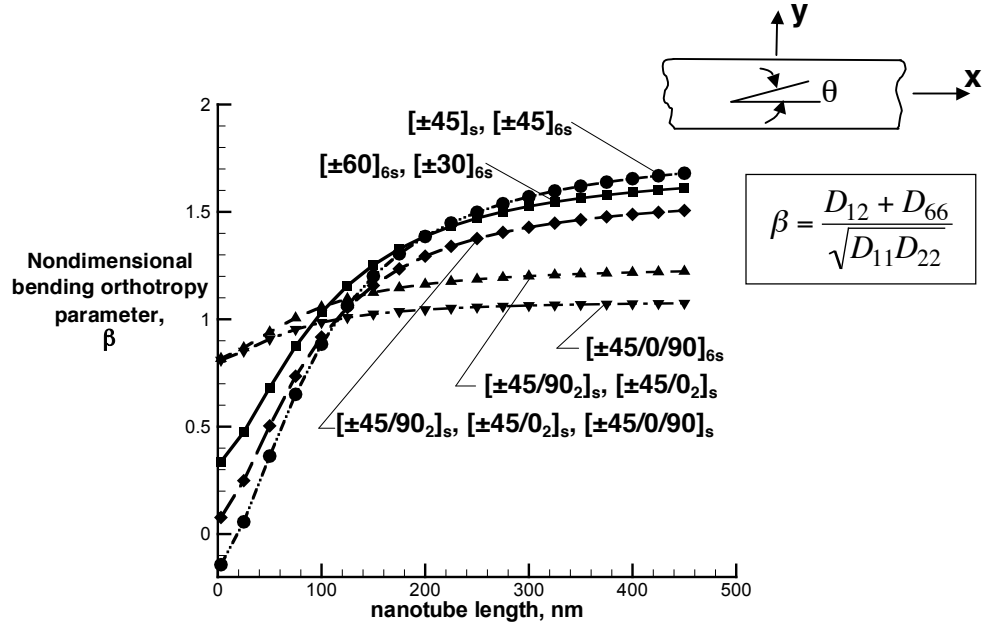(a) 1% nanotube volume fraction

(b) 400-nm nanotube length

Figure 5. Effect of aligned, non-functionalized nanotube length and volume fraction on the non-dimensional bending orthotropy parameter, β, for selected laminates.

$$K_x = \frac{N_x^{cr} b^2}{\pi^2 \sqrt{D_{11} D_{22}}}$$

$$K_s = \frac{N_{xy}^{cr} b^2}{\pi^2 \sqrt{D_{11} D_{22}}}$$

(a) 1% nanotube volume fraction
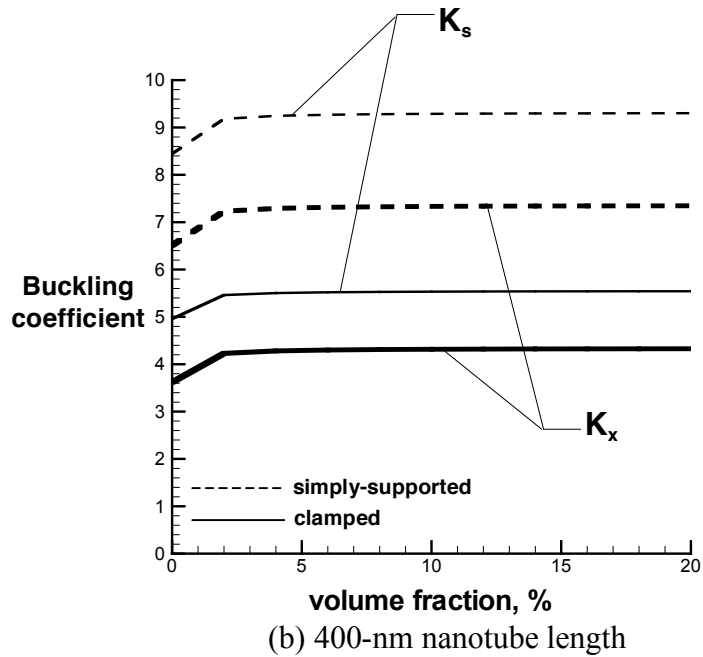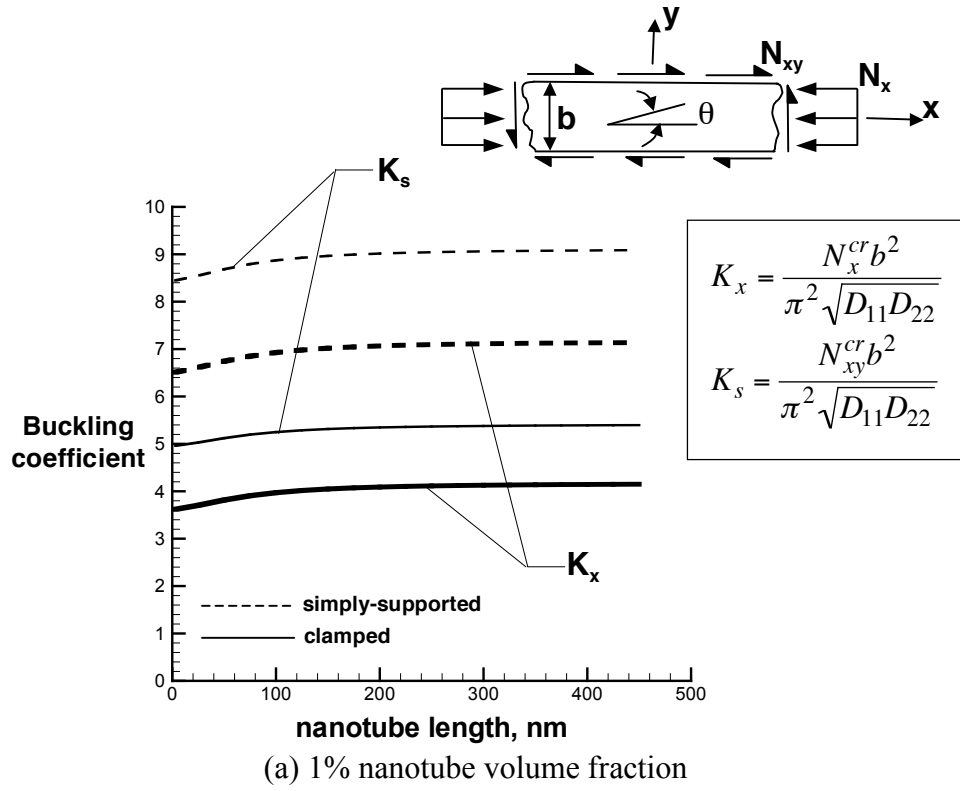
(b) 400-nm nanotube length

Figure 6. Effect of aligned, non-functionalized nanotube length and volume fraction on the non-dimensional buckling coefficients, K_x and K_s, for $[\pm 45/0/90]_{6s}$ laminates subjected to axial compression and shear loadings.

$$K_x = \frac{N_x^{cr} b^2}{\pi^2 \sqrt{D_{11} D_{22}}}$$
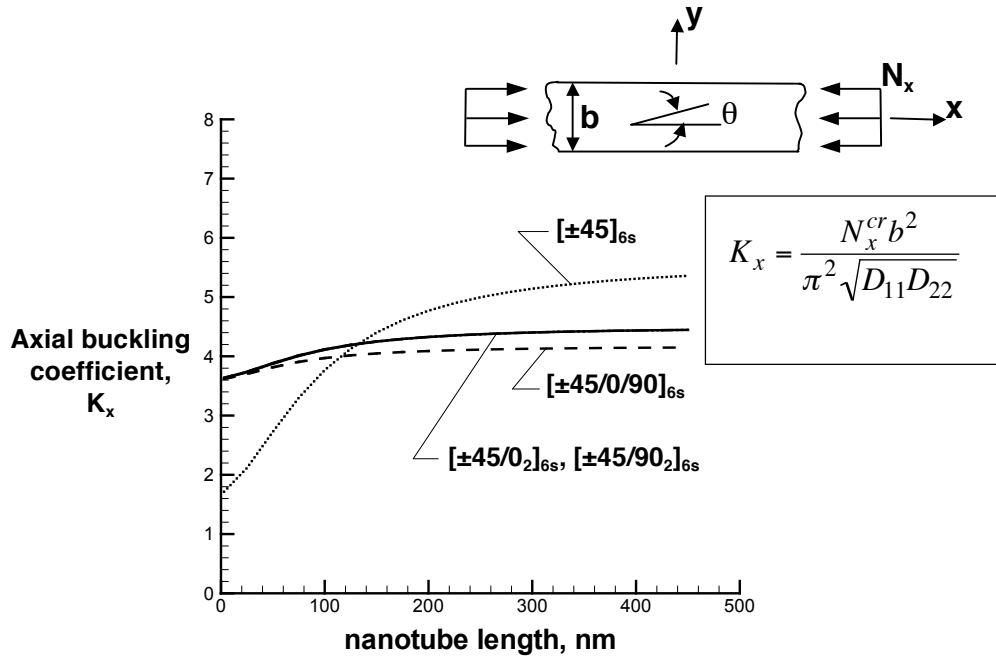
(a) 1% nanotube volume fraction

Figure 7. Effect of aligned, non-functionalized nanotube length on the non-dimensional axial buckling coefficient K_x for selected laminates subjected to axial compression loadings with simply-supported boundary conditions.

$$K_s = \frac{N_{xy}^{cr} b^2}{\pi^2 \sqrt{D_{11} D_{22}}}$$
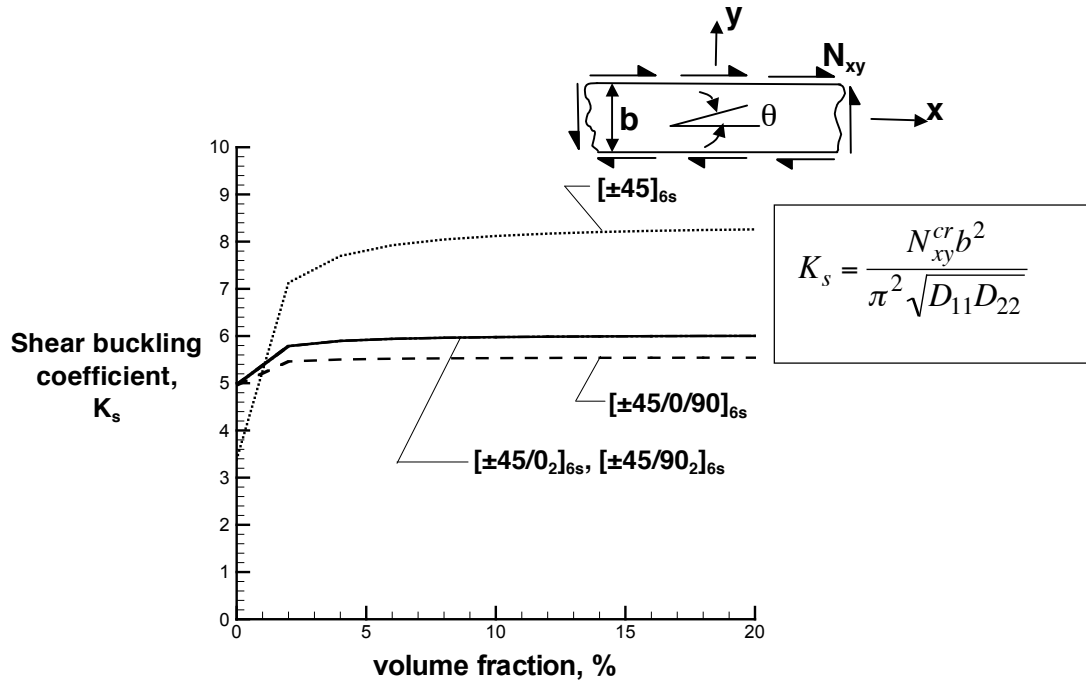
(b) 400-nm nanotube length

Figure 8. Effect of aligned, non-functionalized nanotube volume fraction on the non-dimensional shear buckling coefficient K_s for selected laminates subjected to shear loadings with simply-supported boundary conditions.

Laminate 1: $[(\pm 45/0/90)_3^{L=10nm}/(\pm 45/0/90)_3^{L=\lambda}]_s$

Laminate 2: $[(\pm 45/0/90)_3^{L=400nm}/(\pm 45/0/90)_3^{L=\lambda}]_s$

Laminate 3: $[(\pm 45/0/90)_3^{L=\lambda}/(\pm 45/0/90)_3^{L=400nm}]_s$

Laminate 4: $[(\pm 45/0/90)_3^{L=\lambda}/(\pm 45/0/90)_3^{L=10nm}]_s$

$[\pm 45/0/90]_{6s}$

Normalized ratio of buckling load-to-nanotube weight percent

nanotube length, nm (λ)

(a) 1% nanotube volume fraction

Laminate 5: $[(\pm 45/0/90)_3^{vf=1\%}/(\pm 45/0/90)_3^{vf=\phi}]_s$

Laminate 6: $[(\pm 45/0/90)_3^{vf=10\%}/(\pm 45/0/90)_3^{vf=\phi}]_s$

Laminate 7: $[(\pm 45/0/90)_3^{vf=\phi}/(\pm 45/0/90)_3^{vf=10\%}]_s$

Laminate 8: $[(\pm 45/0/90)_3^{vf=\phi}/(\pm 45/0/90)_3^{vf=1\%}]_s$

$[\pm 45/0/90]_{6s}$

Normalized ratio of buckling load-to-nanotube weight percent

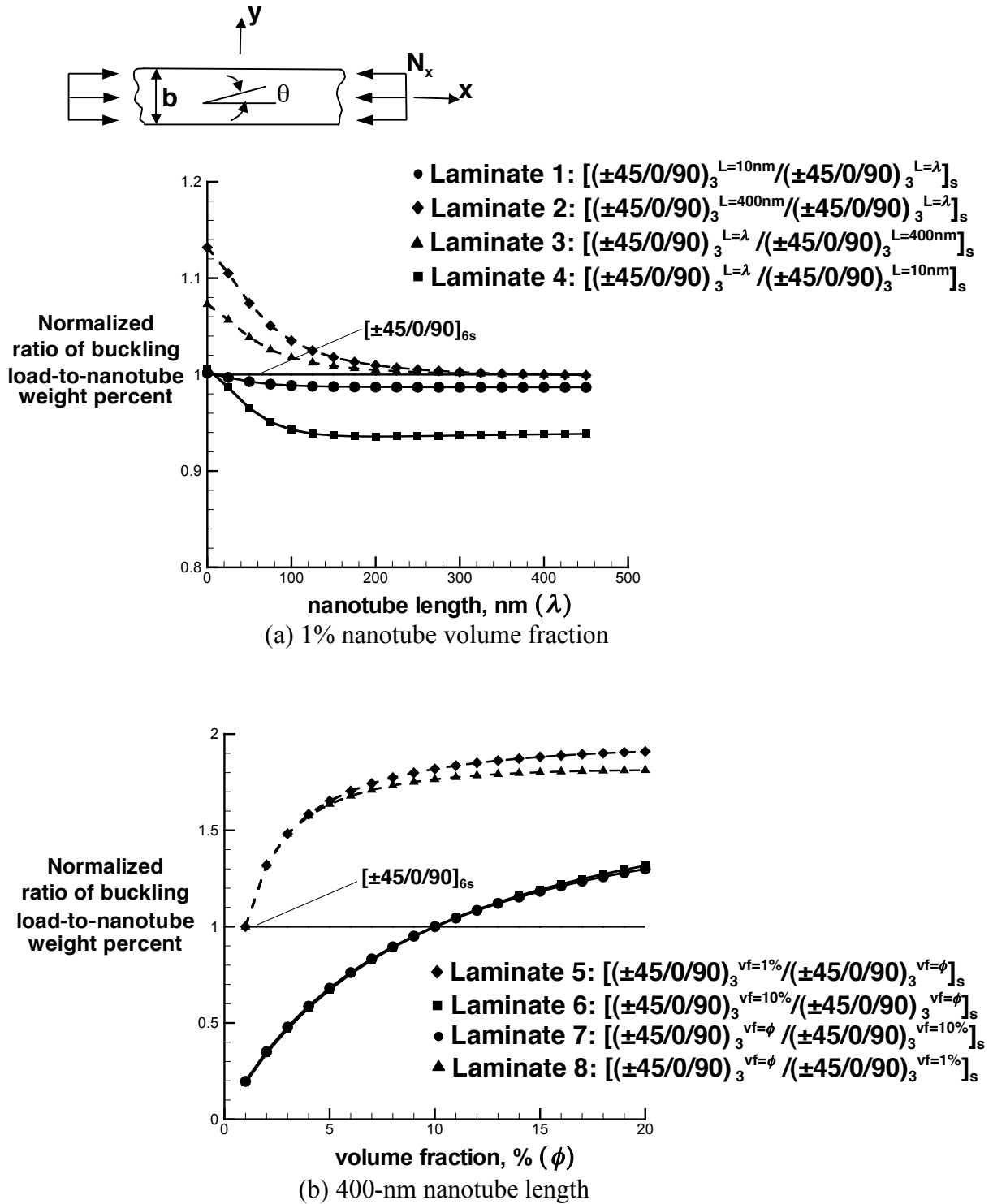**volume fraction, % (ϕ)**

(b) 400-nm nanotube length

Figure 9. Effect of hybrid laminate construction on the ratio of axial buckling load-to-nanotube weight percent for aligned, non-functionalized quasi-isotropic laminates subjected to axial compression loadings with simply-supported boundary conditions.